

# MICP-L: Fast parallel simulative Range Sensor to Mesh registration for Robot Localization

Preprint submitted to ICRA 2023

Alexander Mock<sup>1</sup>, Sebastian Pütz<sup>2</sup>, Thomas Wiemann<sup>1,2</sup> and Joachim Hertzberg<sup>1,2</sup>

**Abstract**—Triangle mesh-based maps have proven to be a powerful 3D representation of the environment, allowing robots to navigate using universal methods, indoors as well as in challenging outdoor environments with tunnels, hills and varying slopes. However, any robot that navigates autonomously necessarily requires stable, accurate, and continuous localization in such a mesh map where it plans its paths and missions. We present MICP-L, a novel and very fast *Mesh ICP Localization* method that can register one or more range sensors directly on a triangle mesh map to continuously localize a robot, determining its 6D pose in the map. Correspondences between a range sensor and the mesh are found through simulations accelerated with the latest RTX hardware. With MICP-L, a correction can be performed quickly and in parallel even with combined data from different range sensor models. With this work, we aim to significantly advance the development in the field of mesh-based environment representation for autonomous robotic applications. MICP-L is open source and fully integrated with ROS and tf.

## I. INTRODUCTION

Localization is the task of estimating the state of a mobile robot in a reference coordinate system. It is required for any mobile robot that autonomously executes its plans in its environment. For example, autonomous driving fleets of agricultural robots rely heavily on accurate GPS measurements to successfully execute their plans in the fields. However, in areas where GPS measurements are rarely available with some accuracy or not available at all, other state estimation strategies need to be considered. Therefore, algorithms such as SLAM have been further developed so that robots are able to simultaneously localize and map their environment. In recent years, these SLAM algorithms have been improved such that even robots with low computational resources have been able to estimate their state in 6DoF while simultaneously mapping their environment as TSDF volumes. These TSDF volumes can be optimized into 3D triangle meshes to compress the information needed to accurately map the environment.

Recently, algorithms for navigating mobile robots on triangle meshes have been developed where the triangle mesh is interpreted as a 2D manifold to efficiently compute paths or complete goal-oriented continuous vector fields directly over the surface and without modifying or refining the mesh [1].

<sup>1</sup>Knowledge Based Systems Group, Institute of Computer Science, Osnabrück University, Berghoffstraße 11, 49090 Osnabrück, Germany amock@uos.de, twiemann@uos.de

<sup>2</sup>DFKI Robotics Innovation Center, Osnabrück branch, Berghoffstraße 11, 49090 Osnabrück, Germany joachim.hertzberg@dfki.de

The DFKI Niedersachsen Lab (DFKI NI) is sponsored by the Ministry of Science and Culture of Lower Saxony and the VolkswagenStiftung



Fig. 1: The Lero agricultural monitoring robot uses MICP-L for localization while performing mesh navigation over beds in a market garden microfarming environment.

Such geodesic path planners are able to compute the shortest path over the surface of a mesh instead of planning over the edges to a specific goal pose. However, a robot needs continuous localization in these maps to follow the computed paths even when a map already exists, i.e. without SLAM. In this paper, we present the novel approach MICP-L to localize a robot equipped with arbitrary range sensors directly in these triangle mesh maps. We place particular emphasis on the ability of our software to run directly on robots with different computational capabilities. Thus, MICP-L is fully integrated with ROS, tf and runs with the ROS mesh navigation stack<sup>1</sup>.

In addition to core localization, we have designed our software to meet the following requirements.

- Lightweight, accurate and fast
- Executable on many computing devices
- Supporting various range sensor models
- Robustness against dynamic obstacles

In the following section, we describe related approaches and the state of the art. Then, we describe our proposed algorithm and corresponding implementation in detail. In the experiments, we show that the software satisfies the above predefined design goals. We also analyze how accurately our software performs in real-world scenarios. As shown in Fig 1,

<sup>1</sup>[https://github.com/uos/mesh\\_navigation](https://github.com/uos/mesh_navigation)

for example, MICP-L is used for localization on a mesh map for our developed monitoring robot Lero while it drives over vegetable beds in a microfarming testbed.

## II. RELATED WORK

In the last decades, 3D map formats has established as improvement to commonly used 2D maps. These 3D maps are often implemented as pointcloud maps. Many researchers contributed SLAM software that can automatically generate these pointcloud maps, for example, LeGO-LOAM [2] or LIO-SAM [3]. For pose tracking, these pointset based SLAM approaches always rely on pointset to pointset registration algorithms, such as GICP [4], as both the model and the sensor data are a set of points. Since points are indefinite small, pointcloud maps tend to be very space consuming and therefore needs to be compressed to e.g. voxel maps [5]. Using voxel maps, however, reduces the accuracy since the space must be discretized. Another method is to reconstruct the point clouds into triangle meshes. These have a much higher compression level and represent the actual environment more accurately than voxel grids, since they do not discretize with voxels but fit surfaces to the data. In the last years it became possible to generate these mesh maps online even on SoC devices [6] and in large scales [7]. Because of their properties of having a closed surface, they are used to plan and execute paths of autonomously driving robots in unstructured environments [1]. This mesh navigation software relies on a stable and frequent localization of the robot relative to the map on which the navigation plans are computed and executed. There are many approaches evolving from Computer Graphics to match point sets to triangle meshes [8], but they were not adapted to a real robotic application in a stable manner. Therefore, we contribute a novel algorithm for direct range sensor to mesh registration by the means of simulating, called MICP-L.

## III. ALGORITHM

Mesh Iterative Closest Points Localization (short: MICP-L) requires data from a range sensor, an initial pose guess, and a triangle mesh map. The general workflow is as follows

- 1) Find correspondences between scan and map
- 2) Estimate  $\Delta T$  of corresponding pointsets
- 3) Apply  $\Delta T$  to pose guess. Repeat with 1)

The proceeding is very similar to classical algorithms of the ICP category. Our contribution, however, is a novel strategy for correspondence finding between scans and meshes.

### A. Simulative Projective Correspondences

We first transform each range sensor measurement  $i$  into a ray representation which consists of an origin  $o_i$ , a direction  $d_i$ , and a range  $r_i$ . For each ray  $i$  we simulate a virtual ray along  $o_i$  and  $d_i$  given a pose estimate. The intersection with the map represents the actual point that would be measured if the sensor were at the estimated pose. The Cartesian point of the real scan measurement is than projected onto the plane of intersection which gives the map correspondence. We call this type of correspondences Simulative Projective

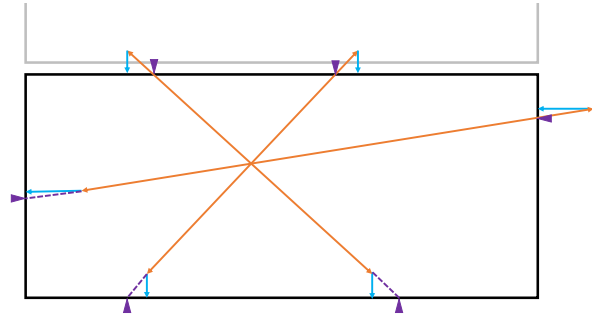


Fig. 2: A 2D map consists of two rooms. With SPC, the real measurement's (orange) correspondences are found using raycasts in the map (purple) and projecting the real measurements onto the intersection plane (blue).

Correspondences (SPC). The concept of SPC is visualized in 2D in Fig. 2. SPC finds map correspondences only in the nearest vicinity and not, for example, in adjacent rooms of the map. This reduces the probability of drifting completely into other rooms during the subsequent correction. Thus, SPC results in stable correspondences consisting of scan points  $s$  and map points  $m$ , where a scan point  $s_i$  is corresponding to the map point  $m_i$ .

### B. Correction

Next, we search for the transformation parameters  $\Delta T$ , consisting of a rotation  $\Delta R$  and a translation  $\Delta t$ , that fit the scan points  $s$  to the map points  $m$  best. This can be done by minimizing the following equation.

$$E(\Delta R, \Delta t) = \frac{1}{n} \sum_{i=1}^n \|m_i - (\Delta R s_i + \Delta t)\|_2^2 \quad (1)$$

As solution to this, we adapt the least square estimation according to Umeyama [9]. Instead of using the mean values of the scan and model points, we use the origin  $o_b$  of the robot base to calculate the covariance matrix  $C$ .

$$C = \frac{1}{n} \sum_{i=1}^n (m_i - o_b)(s_i - o_b)^T \quad (2)$$

From that we perform a singular value decomposition (SVD) to extract the rotational components from the covariance matrix.

$$C = U \Sigma V^T \quad (3)$$

With the mean values of the scan  $\bar{s}$  and the map points  $\bar{m}$  we get the final transformation parameters  $\Delta R$  and  $\Delta t$ .

$$\Delta R = UV^T \quad \Delta t = \bar{m} - R\bar{s} \quad (4)$$

After correcting the pose guess, the steps of SPC and Correction are repeated until convergence. The whole loop of SPC and correction gives the Mesh ICP algorithm (MICP).

### C. Combined Correction

With the approach of Umeiyama and our modifications it is also possible to combine several range sensors and compute an unified correction for them. Given a sensor  $i$  and its covariance matrix  $C_i$  the combined  $C_c$  of all sensors can be calculated by the weighted average, since the covariances are computed around the same center  $o_b$ .

$$C_c = \sum_{i=1}^N w_i C_i \quad (5)$$

The combined means  $\bar{m}_c$  and  $\bar{s}_c$  can be computed accordingly. As long as  $\sum w_i = 1$  applies the weights  $w_i$  can be varied freely, e.g. to give certain sensors more weight than others during correction. If every sensor measurement of each sensor is equally reliable we propose to choose the weights by the number of correspondences  $n_i$ :

$$w_i = \frac{n_i}{\sum n_i} \quad (6)$$

A sensor with many measurements is thus automatically assigned a higher weight than a sensor with fewer measurements. After the covariances of the individual sensors have been combined, the transformation components can be determined as before to obtain a total correction  $\Delta T$ .

## IV. IMPLEMENTATION

Our implementation is integrated into the mesh localization library called *RMCL*<sup>2</sup>. For SPC we use Rmagine as raycasting backend [10]. It is a C++ simulation library particularly designed to develop simulative algorithms running directly on a robots hardware. We split our implementation into modules dependent on the Rmagine simulation backend. It allows the robot to choose at runtime whether to run the algorithm on its CPU or its NVidia GPU. This can be used to flexibly distribute the computational load evenly among the devices and, for example, to react to other computational loads.

### A. MICP-L

For one correction step consisting of SPC, covariance computation, and correction we use classes named after the sensor type  $X$  and the Rmagine backend  $Y$ :  $X$ Corrector $Y$ . For each sensor model  $X$  of Rmagine there is a corresponding MICP-L Corrector implementation. For example, to correct LiDAR measurements via the Rmagine Embree (CPU) backend, a `SphereCorrectorEmbree` must be used. After instantiating a MICP-L corrector, it must be assigned the respective sensor model parameters as well as a map in which the corrector can compute the SPC. Both the map and the sensor model can be modified during runtime and set again. If many sensors share a same robot base, a transformation between the sensor and the base  $T_{sb}$  can be set on the Corrector. Then the Corrector class provides the function `correct` for a complete correction and `compute_covs` to only compute the intermediate covariances, which can

<sup>2</sup>RMCL is released under BSD 3-Clause license and available at <https://github.com/uos/rmcl>.

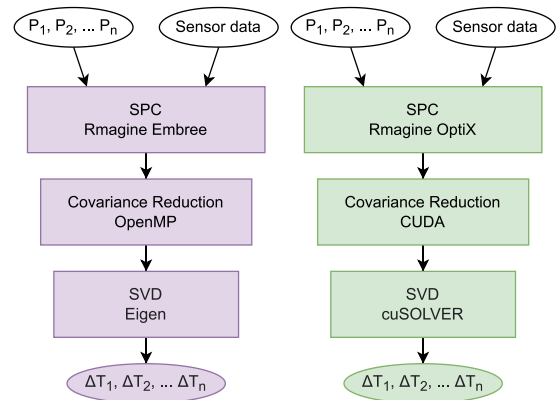


Fig. 3: Workflow of MICP-L Correctors. CPU and GPU computations are colored in green and purple respectively. Both the GPU and the CPU implementation receive a list of pose estimations as inputs as well as sensor data. The outputs are a delta transform for each input pose.

be used e.g. when many sensors are to be combined for correction. Both of these function receive a list of poses on which the correction or the covariances are computed in parallel. For each pose the intersections with the map are computed by Rmagine. The normals at intersection are then used to compute the SPC. In our implementation, we also introduce a parameter to discard correspondences of high simulative projective distances. A partial covariance matrix is then calculated for each valid correspondence. After processing an entire sensor, the partial covariance matrices are reduced to one. This reduction is done either on CPU via OpenMP function or on GPU using CUDA kernels. From the covariance matrices the transformation parameters are obtained either by Eigen's SVD or CUDA's cuSOLVER. For OptiX Correctors, both input and output are CUDA buffers, while for Embree Correctors, both input and output are located in the CPU's RAM. This allows the development of pre- and post-processing steps where data is copied only on demand to ensure maximum performance. The complete workflow of both the CPU and the GPU correction is shown in Fig. 3.

### B. Sensor combination

Our algorithm allows the correction of multiple sensor sources by merging the intermediate covariances of each sensor into one. To access the covariances the function `compute_covs` has to be called on any sensors Corrector object first. We provide functions to combine the covariances into one, either uniformly considering the number of measurements or completely user-defined by freely choosing the weights for each sensor. To better understand which sensors can be used and how they can be combined for correction, an example follows. We want to localize a robot in a 3D map. This robot is only equipped with a 2D LiDAR, which makes hard to estimate its exact 6DoF pose in the map. However, we know that our robot is on the ground most of the time. We can use this information to attach an additional virtual scanner as Rmagine OnDn model to the robot that permanently scans from the wheel centers to the ground. This virtual scanner

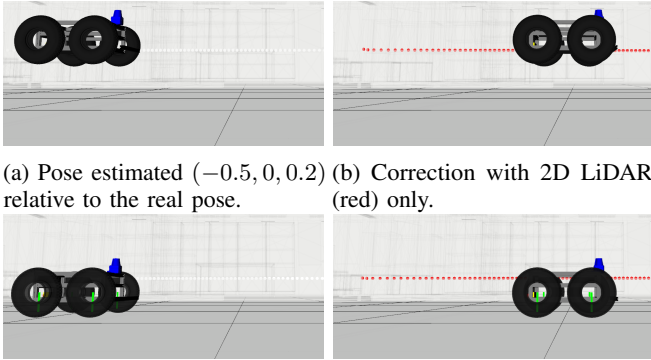


Fig. 4: Visualization of a combined correction until convergence. a) shows the pose guess from which the correction starts. It is approximately 0.2 m over the ground (z) and -0.5 m in x direction of the real pose. b) shows the correction results using only a 2D LiDAR. Here, the robot cannot correct the z error. d) shows the combined correction results considering the single corrections of b) and c) by combining two covariances.

generates fixed distances the size of the wheel radius. Using this virtual scanner and the 2D LiDAR measurements we can built two covariance matrices for a given pose estimate. After reducing the covariances to a single one, the combined correction can be determined, as visualized in Fig. 4.

### C. ROS Integration

With our ROS package we provide a range of code examples using different sensor combinations and computing the corrections either on CPU or on GPU. Via existing ROS sensor drivers existing sensor data can be connected to MICP-L in order to localize a real robot in a given 3d map. Each of MICP-L’s code samples is named after the sensor model and the backend it operates on. Each node subscribes to one ore multiple sensor data topics, corrects the robot at a given update rate, and results in a localization provided as a continuously broadcasted transformation between the robots base and the map via ROS-TF. However, if the robot already has an odometry frame above the base frame, this transformation would break ROS-TF. In this case, MICP-L computes the transformation between the robot’s odometry frame and the map frame instead.

### D. Compatibility

MICP-L depends on Rmagine and ROS and therefore inherits their device installation compatibility. This means that MICP-L can be installed on any computing device where Rmagine and ROS can be installed. The actual implementation of MICP-L and our MICP-L code samples can localize a robot equipped with various range sensors. Examples for these sensors supported by MICP-L are listed in Tab. I. Overall, MICP-L can use any range sensor for localization by integrating Rmagine’s OnDn model, in which each ray can be modeled individually.

TABLE I: List of well known sensors that can be used as sensor source for MICP-L localization.

Model	Sensors
Spherical	Velodyne VLP-16, VLP-32, Ouster OS-0, OS-1, OS-2
Pinhole	MS Kinect, Asus Xtion, Intel RealSense D400 series
OIDn	Livox Mid-40, Avia
OnDn	Custom, virtual

TABLE II: Computers used for evaluation.

Name	CPU	GPU
DPC	AMD Ryzen 7 3700X	NVIDIA RTX 2070 SUPER
NUC	Intel i7 1165G7	NVIDIA RTX 2060 Max-P
LX1	Intel i7 8750H	NVIDIA GTX 1050 Ti Max-Q

## V. EXPERIMENTS

In our experiments we analyze and evaluate our given software according to our preset requirements. Furthermore, we give a detailed overview of what the software is capable of and where its limits are.

### A. Runtime

Next, we analyze the runtime of our GPU and CPU implementation, considering varying map sizes, and different computing devices. The computers used in experiments are listed in Tab. II. For any of the experiments of Fig. 5 we measured the runtime using a Velodyne VLP-16 as sensor. The Velodyne VLP-16 LiDAR sensor has 16 scan lines and operates with framerate up to 20 Hz. In horizontal direction the number of points are adjustable. In our experiments, we set the number of horizontal points to 900, which leads to a total number of 14400 raycasts needed to calculate the SPC. In our performance experiment we spawned 1000 random pose guesses inside an automatically generated sphere. At the sphere’s center we simulated a Velodyne VLP-16 scan. We then used MICP-L to register this scan from each pose estimate against the sphere, so that each random pose estimate finally converges at the center of the sphere. We measured the runtimes per correction step for different number of sphere

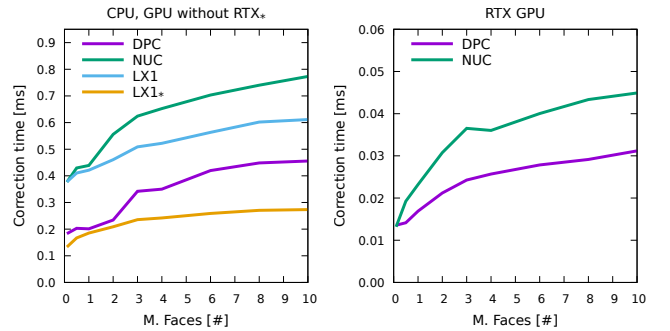


Fig. 5: Runtime evaluation of a single MICP-L iteration in synthetic maps of varying sizes on the different architectures. The left plot shows the runtime measurements of the CPUs and GPUs without RTX graphics card. The right plot shows the runtimes of the GPUs with RTX hardware acceleration.

TABLE III: MICP-L partial runtimes.

Device	Simulation	Reduction	SVD
NUC (CPU)	96.400%	3.586%	0.014%
NUC (GPU)	80.337%	0.376%	19.287%
LX1 (GPU)	94.090%	0.014%	5.896%

triangles. We repeated the experiments for our test devices of Tab. II. The results are shown in Fig. 5. The experiments show our proposed algorithm is capable of being used online even in 3d maps consisting of a large number of triangles. With the Intel NUC’s RTX acceleration, a VLP-16 scan could be corrected about 850,000 times in a map of 1 million faces, before the next scan is taken.

As second experiment we measured each component of MICP-L (Fig. 3) of both the CPU and GPU implementation spawning a sphere consisting of 1M faces and registering 1000 poses against the mesh. The results in Tab. III give an overview of how much time each fraction of the correction needs in relation to the entire computation.

### B. Accuracy

In this section we perform experiments to show the accuracy of MICP-L. For our experiments, we used a simulated Gazebo world called AVZ, which is available online via the ROS package uos tools. In this way, we can obtain a map that perfectly matches the environment and exclude the factor of the erroneous map in the accuracy analysis. In the simulated world we placed a ceres robot equipped with a Velodyne VLP-16 and applied Gaussian noise to the simulated LiDAR data with a standard deviation of 0.8 cm. In the first experiment we run MICP-L giving a stationary robot a pose guess near its real position. It converged to a translation error of 0.01967 cm. The fact that the error is smaller than the sensor inaccuracy can be justified by the fact that the individual errors average out on the surfaces during registration. The next experiment the robot moves through the simulated AVZ environment. From two test drives we extracted the ground truth trajectories directly from Gazebo as shown in Fig. 6. From the wheel revolutions we estimated a simple but inaccurate odometry estimation. We let MICP-L continuously correct this odometry estimation to the mesh. Both the standalone odometry estimation and the MICP localization we compared to the ground truth. The mean errors (ME) are listed in Tab. IV. The results show that MICP-L is able to correct the inaccurate odometry estimate,



Fig. 6: Two test drives in Gazebo AVZ world. The ground truth trajectories are colored in red and blue.

TABLE IV: Mean Error (ME) in meters of the Odometry estimation and MICP-L in the test drives of Fig. 6.

Drive	Odometry ME [m]	MICP-L ME [m]
red	8.2280	0.0098
blue	4.5485	0.0086

achieving an average accuracy of about 1 cm.

### C. Real-World Performance

In this section we perform experiments to visualize the performance of MICP-L in real world scenarios. For that we installed our software on two robots.

1) *Indoors - Perceptibot*: In the first indoor scenario we installed MICP-L on the Perceptibot robot and scanned our office building with a Riegl VZ-400i terrestrial laser scanner as shown in Fig. 7. The Perceptibot has a differential drive and is equipped with a Velodyne VLP-16 range sensor. Since it only has an Intel NUC computer without a GPU, the following experiments were performed with the CPU implementation of MICP-L. In both test drives, we manually controlled the robot through the central room of the office building. The robot was always steered to the same place where it had started its drive. In the first drive, all doors were closed and no obstacles were present, exactly matching the robots map. In the second drive, however, we opened all doors and frequently walked into its sight. The trajectories estimated by MICP-L are shown in Fig. 8. As orientation we added the trajectories of the robot’s odometry estimations as well. The odometry is estimated by an EKF that fuses odometry of the wheel encoders and IMU measurements. The results show that MICP-L estimates the robots pose with high precision. In contrast to the EKF trajectory the gaps at start and end are closed. Even in the second experiment with obstacles and an environment that does not completely match the robot’s map, MICP-L successfully localizes the robot.

2) *Outdoors - Lero*: In this part, we investigate the localization of our approach outdoors using the agricultural monitoring robot Lero. This is designed for use in market gardens, microfarming as shown in Fig 9. Lero is equipped with a Ouster OS1-64 LiDAR that is used for MICP-L. Furthermore, Lero has two Intel NUCs as computers both capable of hardware accelerating MICP-L with their RTX GPUs. The Intel NUC model is listed in Tab. II.

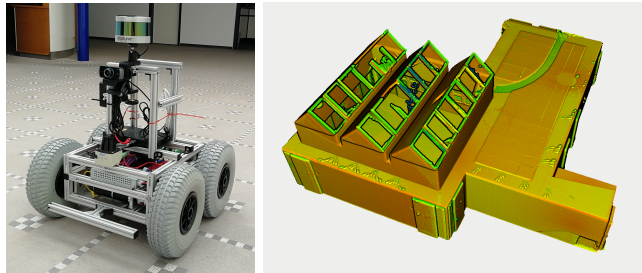


Fig. 7: Perceptibot (left) stands in an office building scanned in high resolution (right).

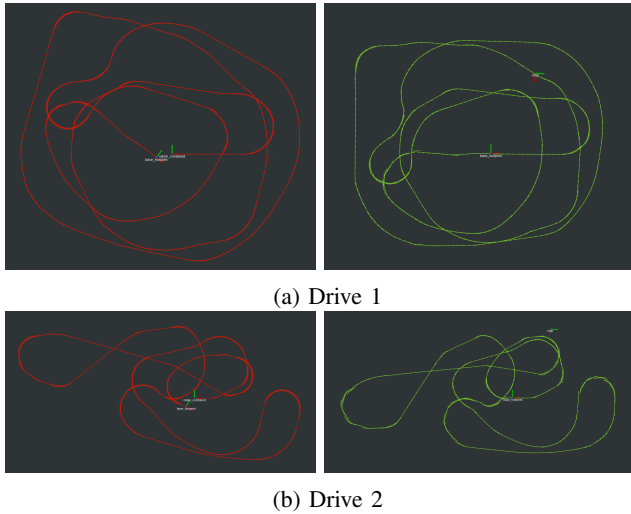


Fig. 8: Perceptibot: Trajectories of two indoor drives. Red is the trajectory of the odometry estimated by an EKF. Green is the trajectory of MICP-L.



Fig. 9: Lero: agricultural monitoring robot.

The environment of the following experiments was previously recorded and reconstructed to a triangle mesh as shown in Fig. 1. There are many beds with a width of about 75 cm, usually 10 meters long, and a track width of one meter next to each other. In such outdoor semi and unstructured environments, navigation on 2D maps, such as occupancy grid maps is limited feasible or suboptimal. For robot navigation, 3D Occupancy Gridmaps are also of limited use, as they cannot be used for surface shortest path computation, as described in [11]. Instead, we use the Continuous Vector Field Planner (CVP) [1], which is a vector field and path planner developed explicitly for meshes. This planner is part of the mesh navigation stack, which is integrated with the middle layer navigation framework Move Base Flex [12].

We further recorded three test drives, showing the mentioned mesh navigation method in combination with the presented localization approach MICP-L. The trajectories estimated by MICP-L, the EKF, and a RTK-GPS module is shown in Fig. 10. Since the GPS data showed large uncertainties in some places, we refrain here from a more detailed analysis of the localization accuracy. However, we observed that Lero was able to robustly navigate across the field to a goal in front of a field entry and stand there so precisely that he could steer through the beds afterwards.

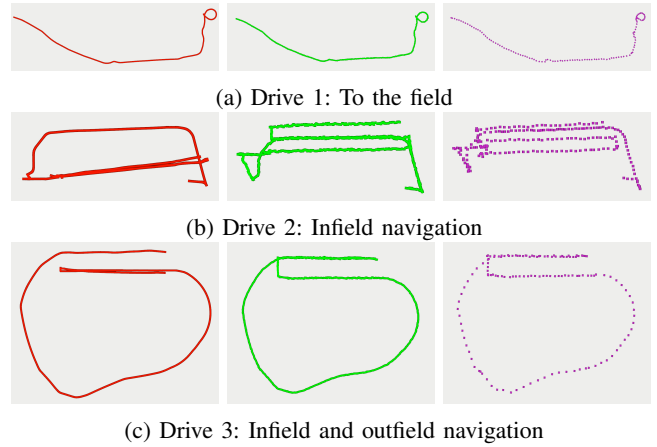


Fig. 10: Outdoor experiments navigating the agricultural monitoring robot Lero on a field. For each of the drives a), b), and c) we recorded the trajectory of the EKF (red), MICP-L (green), and a RTK-GPS (purple).

## VI. CONCLUSION AND FUTURE WORK

We presented MICP-L, a novel approach to directly localize a robot equipped with one or more range sensors in a triangle mesh map. After providing an initial pose guess and range data of a real range sensor, we use RTX accelerated ray simulations to compute the SPC with the mesh. The SPC are then used to iteratively correct the pose guess. Dependent on the robots hardware capabilities, MICP-L can be executed either on CPU or GPU. If the robot has both CPU and GPU, the developer can flexibly distribute workloads. MICP-L can be used with a wide range of commonly used range sensors.

We evaluated the runtime on different devices and tested MICP-L in real-world scenarios; indoors and outdoors. With the outdoor experiments we showed that approaches as mesh navigation actually benefit from MICP-L localization. Future work will investigate what information can be transferred from the map to the sensor data once the robot is localized. For example, a localized robot can separate the scan points that belong to the map from the other points. This automatically gives a pre-segmentation for obstacle or human detection algorithms as showed in Fig. 11.

Because of the MICP-L's correction speed, future work will also deal with integrating this approach into a particle filter.

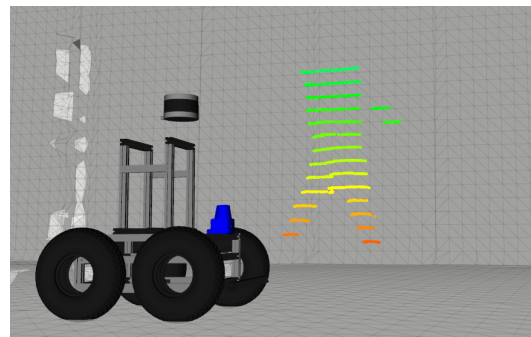


Fig. 11: VLP-16 Segmentation after MICP localization.

## REFERENCES

- [1] S. Pütz, T. Wiemann, M. Kleine Piening, and J. Hertzberg, “Continuous shortest path vector field navigation on 3d triangular meshes for mobile robots,” in *2021 IEEE International Conference on Robotics and Automation (ICRA)*, 2021. [Online]. Available: [https://github.com/uos/mesh\\_navigation](https://github.com/uos/mesh_navigation)
- [2] T. Shan and B. Englot, “Lego-loam: Lightweight and ground-optimized lidar odometry and mapping on variable terrain,” in *2018 IEEE/RSJ International Conference on Intelligent Robots and Systems (IROS)*. IEEE, 2018, pp. 4758–4765.
- [3] T. Shan, B. Englot, D. Meyers, W. Wang, C. Ratti, and R. Daniela, “Lio-sam: Tightly-coupled lidar inertial odometry via smoothing and mapping,” in *IEEE/RSJ International Conference on Intelligent Robots and Systems (IROS)*. IEEE, 2020, pp. 5135–5142.
- [4] A. Segal, D. Haehnel, and S. Thrun, “Generalized-icp,” in *Robotics: science and systems*, vol. 2, no. 4. Seattle, WA, 2009, p. 435.
- [5] H. Oleynikova, Z. Taylor, M. Fehr, R. Siegwart, and J. Nieto, “Voxblox: Incremental 3d euclidean signed distance fields for on-board map planning,” in *IEEE/RSJ International Conference on Intelligent Robots and Systems (IROS)*, 2017.
- [6] M. Eisoldt, M. Flottmann, J. Gaal, P. Buschermöhle, S. Hinderink, M. Hillmann, A. Nitschmann, P. Hoffmann, T. Wiemann, and M. Porrmann, “Hatsdf slam – hardware-accelerated tsdf slam for reconfigurable socs,” in *2021 European Conference on Mobile Robots (ECMR)*, 2021, pp. 1–7.
- [7] T. Wiemann, I. Mitschke, A. Mock, and J. Hertzberg, “Surface reconstruction from arbitrarily large point clouds,” in *2018 Second IEEE International Conference on Robotic Computing (IRC)*, Jan 2018, pp. 278–281.
- [8] S. Rusinkiewicz and M. Levoy, “Efficient variants of the icp algorithm,” in *Proceedings third international conference on 3-D digital imaging and modeling*. IEEE, 2001, pp. 145–152.
- [9] S. Umeyama, “Least-squares estimation of transformation parameters between two point patterns,” *IEEE Transactions on Pattern Analysis and Machine Intelligence*, vol. 13, no. 4, pp. 376–380, 1991.
- [10] A. Mock, T. Wiemann, and J. Hertzberg, “Rmagine: 3D Range Sensor Simulation in Polygonal Maps via Raytracing for Embedded Hardware on Mobile Robots,” in *2023 IEEE International Conference on Robotics and Automation (ICRA)*, Manuscript submitted. [Online]. Available: <https://github.com/uos/rmagine>
- [11] S. Pütz, “Navigation Control & Path Planning for Autonomous Mobile Robots.” PhD-Thesis, Osnabrück University, Feb. 2022.
- [12] S. Pütz, J. S. Simón, and J. Hertzberg, “Move Base Flex: A highly flexible navigation framework for mobile robots,” in *2018 IEEE/RSJ International Conference on Intelligent Robots and Systems (IROS)*, October 2018. [Online]. Available: [https://github.com/magazino/move\\_base\\_flex](https://github.com/magazino/move_base_flex)